RSC Advances

PAPER

View Article Online
View Journal | View Issue

Cite this: *RSC Adv.*, 2023, **13**, 17536

Digital light processing 3D printing of dynamic magneto-responsive thiol-acrylate composites†

Ines Cazin, [a] Elisabeth Rossegger,[a] Ignazio Roppolo, [b] Marco Sangermano, [b] Petra Granitzer, [c] Klemens Rumpf[c] and Sandra Schlögl *[a]

Additive manufacturing is one of the most promising processing techniques for fabricating customized 3D objects. For the 3D printing of functional and stimuli-triggered devices, interest is steadily growing in processing materials with magnetic properties. Synthesis routes for magneto-responsive soft materials typically involve the dispersion of (nano)particles into a non-magnetic polymer matrix. Above their glass transition temperature, the shape of such composites can be conveniently adjusted by applying an external magnetic field. With their rapid response time, facile controllability, and reversible actuation, magnetically responsive soft materials can be used in the biomedical field (*e.g.* drug delivery, minimally invasive surgery), soft robotics or in electronic applications. Herein, we combine the magnetic response with thermo-activated healability by introducing magnetic Fe_3O_4 nanoparticles into a dynamic photopolymer network, which undergoes thermo-activated bond exchange reactions. The resin is based on a radically curable thiol-acrylate system, whose composition is optimized towards processability *via* digital light processing 3D printing. A mono-functional methacrylate phosphate is applied as a stabilizer to increase the resins' shelf life by preventing thiol-Michael reactions. Once photocured, the organic phosphate further acts as a transesterification catalyst and activates bond exchange reactions at elevated temperature, which render the magneto-active composites mendable and malleable. The healing performance is demonstrated by recovering magnetic and mechanical properties after the thermally triggered mending of 3D-printed structures. We further demonstrate the magnetically driven movement of 3D-printed samples, which gives rise to the potential use of these materials in healable soft devices activated by external magnetic fields.

Received 15th April 2023
Accepted 5th June 2023

DOI: 10.1039/d3ra02504g

rsc.li/rsc-advances

1. Introduction

Since the beginning of the 1980s, 3D printing has become a fast-emerging technology, which has been successfully implemented world-wide in academic and several industrial sectors.[1] Multi-functional objects with complex and customized architectures are easily formed into physical objects by layer-by-layer deposition of materials directly from computer-aided design without molds and heavy machining.[2] Due to freedom in component design and production, the 3D printing technology is applied for fabricating parts used in industrial machines, consumer products (electronics), motor vehicles, and aerospace or medical (dental) sectors.[3] However, significant progress has been achieved by introducing a shape-morphing capability into 3D-printed objects, also known as 4D printing. Initiated and termed by researchers from MIT[4] in collaboration with Stratasys, Inc., the fourth dimension of 3D printed objects offers the ability to switch their geometric configuration in response to variations of the surrounding environment. This unlocks a new toolbox of application areas in 3D printing.[5] Numerous external stimuli can be applied such as light,[6,7] heat,[6,8] temperature,[9] solvent,[10] pH value,[11] electric field,[12] magnetic field[13] or humidity.[14] Due to their multi-functional behavior (*e.g.* reconfigurable structure, shape memory effect, actuation, sensing), these composites can be used in a broad variety of applications[15] including soft robotics,[16] shape memory structures,[17] sensors and actuators.[18]

In this context, great effort has been devoted to develop magneto-active materials for functional composites.[19] By exposure to an external magnetic field, these materials undergo mechanical and rheological changes (*e.g.* damping, elasticity), and shape changes. Magneto-responsive materials are found in the form of a fluid, a gel or a solid.[20] Solid magneto-active materials consist of a soft polymeric matrix, in which inorganic magnetic particles (*e.g.* ferrite particles Fe_3O_4, maghemite γ-Fe_2O_3 or neodymium–iron–boron particles NdFeB)[21] are

[a]*Polymer Competence Center Leoben GmbH, Roseggerstrasse 12, A-8700, Leoben, Austria. E-mail: sandra.schloegl@pccl.at*

[b]*Department of Applied Science and Technology, Politecnico di Torino, Duca degli Abruzzi, 24, 10124, Torino, Italy*

[c]*Institute of Physics, University of Graz, Universitätsplatz 3, 8010, Graz, Austria*

† Electronic supplementary information (ESI) available: FTIR spectra and photographs of printed test structures after testing. See DOI: https://doi.org/10.1039/d3ra02504g

dispersed. Prominent examples of polymers are elastomers,[22] plastomers[23] and foams.[24] A typical behavior of magneto-responsive elastomers (MREs) under the application of a magnetic field is their change of modulus. However, the range of applications is limited due to small magnetically induced actuation strain. Various additive manufacturing techniques, such as direct ink writing (DIW) and fused filament fabrication (FFF) have been employed to fabricate polymers containing high loads of magnetic fillers.[25,26] Colorado and Restrepo demonstrated the printing of an epoxy resin loaded with magnetite particles up to 41 wt% *via* DIW. Results on compressive strength and ductility of tested printed composites showed their applicability in structural components.[27] In 2018, Zhao *et al.* reported the 3D printing of elastomer composites filled with ferromagnetic microparticles prepared by direct ink writing. More precisely, they were able to program ferromagnetic domains in complexly designed 3D-printed materials by applying a magnetic field directly to the dispensing nozzle during the printing process.[28]

Recently, Rodionova *et al.* incorporated magnetic ferrite particles into polylactic acid and produced objects with tunable magnetic properties *via* FFF. Results set up the stage for the additive manufacturing of composites with controlled magnetic anisotropy, as well as, for achieving a spatial distribution of nanofillers in a non-magnetic polymeric matrix.[29] One of the salient feature of DIW is that inks with high loads of magnetic fillers are applicable.[25] Moreover, previous research showed that both DIW and FFF can be used to produce fast responding actuators[30] as well as permanent magnets.[31] Despite the mentioned advantages, objects printed by these techniques suffer from poor resolution. In addition, fillers may be not homogeneously dispersed, which leads to inhomogeneous magnetic response. In addition, high temperatures required during the FFF process may affect the fillers negatively.[32]

Another promising printing approach is based on vat photopolymerization, in which the liquid photo-reactive resin is mixed with magnetic fillers. The method known as digital light processing (DLP) 3D printing is based on a layer-by-layer curing of the resin upon irradiation with a suitable light source. Compared to DIW and FFF, DLP offers several advantages, as it provides higher resolution and build speed, and it operates at room temperature. However, vat photopolymerization presents some drawbacks in terms of the maximum load of fillers in the resin. The photopolymerization process may be negatively affected by an increase in the content of fillers, which compromise on the optical properties of the resin. In addition, the stability and sedimentation of dispersed fillers in the liquid resin plays a vital role in achieving 3D-printed objects with a homogeneous magnetic response. In 2019, Lantean *et al.* developed magneto-responsive photopolymers based on a urethane-acrylate resin filled with Fe_3O_4 nanoparticles. Mechanical properties were tuned by adding butyl acrylate, which reduced the resin's viscosity, and magnetic properties were tailored by loading magnetic filler up to 6 wt%.[33] In subsequent work, the authors studied the magnetically driven self-assembly of Fe_3O_4 nanoparticles into chain-like structures within the vat. The rotation and kinetics of chain formation depended on the viscosity, weight percentage of nanofillers, the intensity of the external magnetic field, and its application time. By applying magnetic fields of varying direction and intensity during the printing process, the authors could control the orientation and the length of the magnetic chains in each printed layer, which was exploited for the fabrication of magnetically driven devices.[34]

Recently, our group demonstrated the possibility to print soft magneto-active objects using thiol-click photopolymers as matrix. In particular, by advancing from pure acrylate to thiol-acrylate systems, we overcome shrinkage stress, oxygen inhibition and low monomer conversion of the filled photopolymers. Soft and flexible polymer composites were obtained by DLP 3D printing with 6 wt% of Fe_3O_4 nanoparticles at a reasonable build time.[35]

Herein, we extended the functionality of 3D printable magneto-responsive thiol-acrylate composites by introducing an additional healing and re-shaping function. In particular, we exploited thermo-activated bond exchange reactions following catalyzed transesterification to induce a material flow above the networks topological freezing temperature. We optimized the composition of the photocurable formulation in terms of viscosity and stability and were able to 3D print objects with a Fe_3O_4 loading of up to 6 wt%. As a proof of concept, magneto-responsive structures were DLP 3D printed, which were thermally healed and could be conveniently reshaped and activated by applying an external magnetic field.

2. Results and discussion

2.1. Network design and optimization of the photocurable resin containing Fe_3O_4 nanofillers

To prepare magnetically responsive dynamic photopolymers, we used our recently reported thiol-acrylate system, which has been loaded with magnetic Fe_3O_4 nanoparticles (d_{50} = 50 nm) as a basis.[36]

The system was composed of hydroxy-2-phenoxypropyl acrylate (**HPPA**) and glycerol 1,3-diglycerolate diacrylate (**GDGDA**) and provided ample –OH groups for the thermo-activated transesterification reaction (Fig. 1).

Trimethylolpropane tri(3-mercaptopropionate) (**TMPMP**) was added as a thiol crosslinker to switch the curing mechanism of pure acrylates following a chain-growth mechanism to a mixed mode one including chain-growth and step-growth reactions. In previous work, we further employed a monofunctional methacrylate phosphate as stabilizer to prevent thiol-Michael reactions and to increase the stability of the photo-curable resins during storage and printing. In another study we showed that this stabilizer is also able to catalyze transesterification reactions due to its Brønsted acidity.[35] Herein, we exploited this feature to print magneto-active composites with additional functions such as thermo-activated mendability.

We varied the filler loading between 0 and 6 wt%, as previous work revealed that filler loadings >6 wt% negatively affect the cure kinetics and stability of the photocurable thiol-acrylate resins. In the present study, we additionally varied the

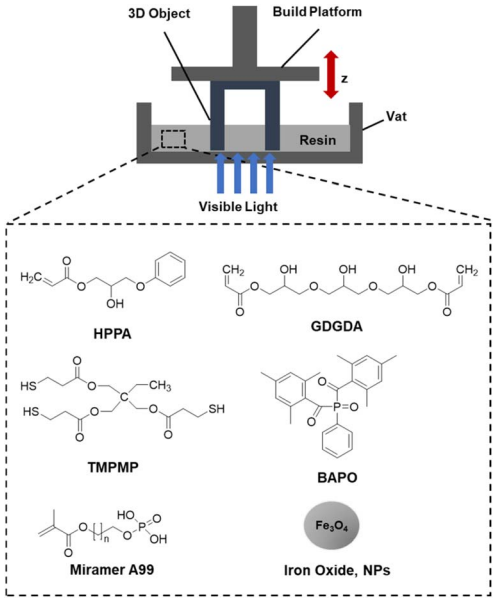

Fig. 1 Monomers, transesterification catalyst, photoinitiator and iron oxide nanoparticles (NPs) used in magneto-responsive resins processed *via* DLP 3D printing.

Table 1 Molar composition of the thiol-acrylate formulations under investigation

Compound	Resin-1 (ref. 36)	Resin-2
HPPA	50 mol%	65 mol%
GDGDA	25 mol%	25 mol%
TMPMP	25 mol%	10 mol%
BAPO	2 wt%	5 wt%
Miramer A99	5 wt%	5 wt%

content of the low viscous **HPPA** and the thiol crosslinker to reduce the viscosity of the formulations and increase the resins' stability, respectively (Table 1).

As viscosity and shelf life of the resin are crucial parameters in vat photopolymerization 3D printing, we determined the viscosity of the new resin formulation (resin-2) with varying content of magnetic nanofillers (0–6 wt%) (Fig. 2b) and compared it with our previously published system (Fig. 2a). The measurements were performed over a prolonged time (15 min) to further get an idea of the resins' stability. Rheological data reveal that the viscosity increases with rising filler concentration but does not exceed 1000 mPa s, which is still within the range (250 and 5000 mPa s) of 3D DLP printable resins.[37]

By increasing the **HPPA** content from 50 mol% to 65 mol% and by decreasing the thiol content from 25 mol% to 10 mol%, the viscosity of the filled and unfilled resins could be significantly reduced. In particular, for the unfilled resin, a decrease in the viscosity from 1320 to 203 mPa s was observed. Interestingly, the addition of up to 4 wt% of nanofillers did not significantly affect the viscosity compared to the unfilled system (302 *versus* 203 mPa s). In contrast, the presence of 6 wt% of nanofillers resulted in a rapid increase in viscosity (934 mPa s) which is also reported for other systems.[38] Due to the reduction of the thiol content in resin-2, the stability of the filled and unfilled compounds could be significantly improved compared to the previously studied resin systems.

In contrast to previous work, we additionally increased the **BAPO** concentration from 2 to 5 wt% to accelerate the cure rate. **BAPO** as a classical radical photoinitiator absorbs in the visible region (λ = 360–440 nm) and forms up to four radicals by undergoing two subsequent Norrish type I reactions across the σ bond between the carbonyl groups and the phosphor atom.[39] Since the formed radicals rapidly initiate radical-mediated polymerization reactions, **BAPO** is a commonly used photoinitiator for the photocuring of acrylate, thiol-acrylate and interpenetrating epoxy-acrylate resins.[40]

We studied the cure kinetics by Fourier-transform infrared (FTIR) spectroscopy, in which the C=C–H stretching band of the acrylate groups was monitored at 1616 and 1634 cm^{-1} upon exposure at 405 nm. It should be pointed out that the IR signal at 2575 cm^{-1}, which belongs to the mercapto groups, was too

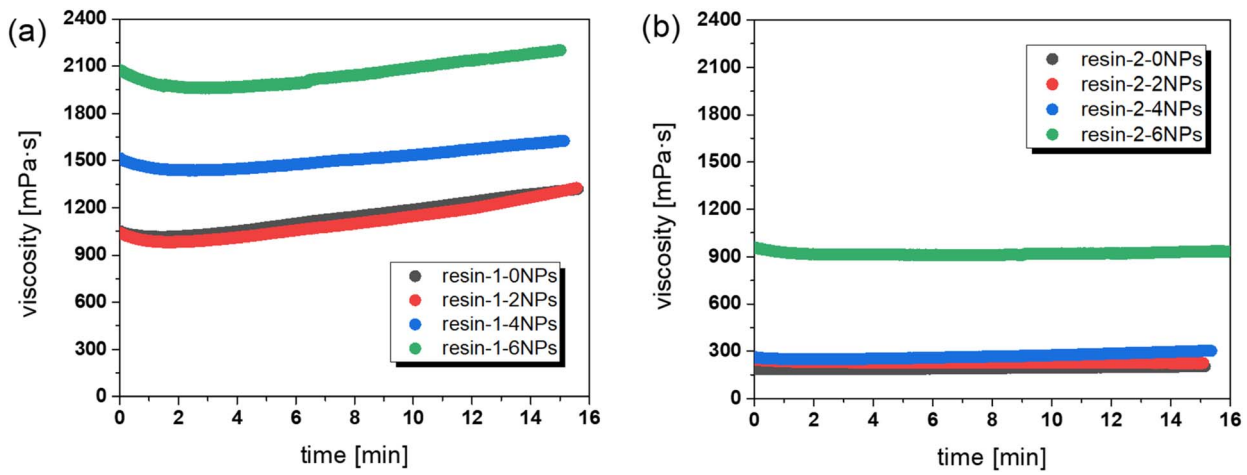

Fig. 2 Stability of the resins filled with up to 6 wt% of nanofiller at a constant shear of 300 s^{-1}: (a) published thiol-acrylate vitrimer system (resin-1)[36] and (b) modified thiol-acrylate vitrimer system (resin-2).

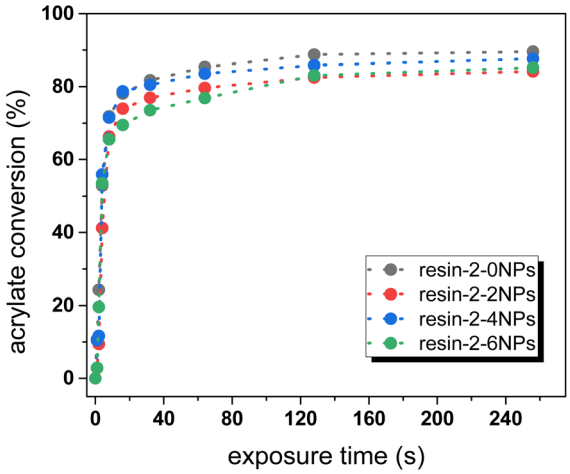

Fig. 3 Monitoring the acrylate conversion of resin-2 as a function of the concentration of Fe_3O_4 nanoparticles. The lines are a guide for the eye.

weak to consider for quantitative evaluation. The IR spectrum of resin-2-0NPs (prior to and after light exposure) is provided in Fig. S1 in ESI.† We studied the acrylate conversion *versus* the filler content as Fe_3O_4 nanoparticles absorb light in the UV and visible region (internal filter effect). The results clearly show that the presence of the nanofillers slows down the reaction kinetics, albeit at a lower extend as expected (Fig. 3). For the unfilled resin, the monomer conversion amounted to 85% after 64 s of light exposure, whilst it decreased to 76% for the system containing 6 wt% filler.

2.2 3D printing and material characterization

Due to the decent cure rates, it was possible to DLP 3D print test specimen for dynamic mechanical thermal analysis (DMTA) and stress relaxation studies. DMTA was used to study the thermo-mechanical properties of the 3D-printed samples filled with nanofillers in the range of 0 to 6 wt% (Fig. 4). When nanoparticles were added to the photocurable formulation, the T_g of the printed composites increased from 45 °C (resin-2-0NPs) to 51 °C (resin-2-6NPs). In previous works, a reduction of the T_g for magneto-responsive nanocomposites based on urethane-acrylate resins was observed and explained by the decrease of the monomer conversion due to competition between the photoinitiator and nanofiller in absorbing radiation during the printing process.[33]

Interestingly, here we observed a slight increase in the T_g value by introducing nanofillers into the system. On the one hand, this can be explained by the presence of the thiol cross-linkers, which lead to higher carbon double bond conversion due to the mixed mode curing mechanism. Thiols act as chain-transfer agents for the chain-growth polymerization of acrylates and reduce the kinetic chain length. This results in lower diffusion limitations of the reacting monomers and a shift of the gel point to higher conversions.[41]

On the other hand, coordinative bonds might be formed between the Fe_3O_4 nanoparticles and the unreacted thiol groups, which anchor the filler to the photopolymer matrix.[35] In the presence of the organic phosphate, the photopolymer composites are able to undergo thermo-activated dynamic bond exchange reactions across the functional –OH and ester groups (transesterification). The change in the viscoelastic properties was studied by rheometer experiments.

Fig. 5 provides the time-dependent evolution of the relaxation modulus for resin-2 with varying concentration of nanofillers at 180 °C. While temperature and catalyst in the thiol-acrylate systems have an impact on the stress relaxation kinetics,[36] the results clearly indicate that the addition of nanofillers (and the related slight shift to higher T_g values) does not significantly affect the bond exchange rate within the investigated range of filler concentration.

2.3 Thermal healing and magnetic properties

Although resin-2 was printed with up to 6 wt% of nanofillers, we performed further printing studies with resin-2-4NPs to avoid premature gelation during the printing process. To demonstrate the magnetic response of the filled thiol-acrylate vitrimer network, a printed stripe was fixed on one side with tweezers. As is shown in Fig. 6a, by applying an external magnetic field (1.24

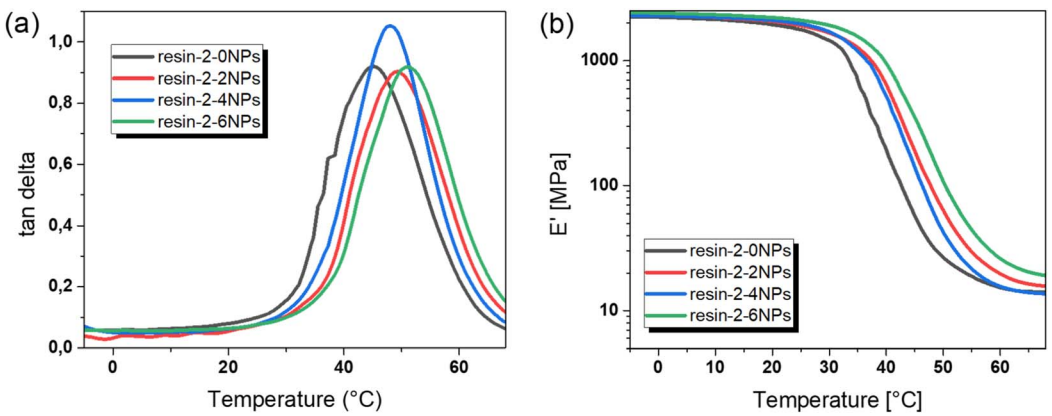

Fig. 4 (a) Loss factor (tan δ) and (b) storage modulus (E') *versus* temperature as obtained from DMA measurements of resin-2 filled with nanofillers up to 6 wt%.

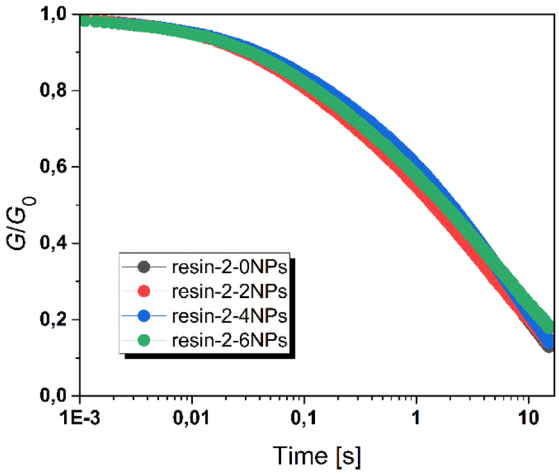

Fig. 5 Normalized stress-relaxation curves (obtained at 180 °C) of resin-2 with varying filler concentration.

T), the stick containing 4 wt% of nanofillers could be activated even without physical contact between the magnet and the stick. Moreover, we printed a stickman where every single part was activated separately. It should be noted that we were not able to print more complex structures as premature gelation occurred at a filler concentration of 4 wt% upon prolonged printing time. In addition, the viscosity of the filled resin was too high to print objects with feature sizes lower than 1 mm.

Thermal healing of magneto-responsive photopolymers was demonstrated on 3D-printed dumbbell test specimens. An appropriate aligning of thin broken test bars is challenging and thus, test bars with a circular-shaped hole in the center were printed together with the circular-shaped counterpart (Fig. 7b).

For the healing step, the disc was fitted in the hole and a thermal healing/welding at 180 °C for 4 h was carried out. Due to the macroscopic reflow, the boundaries between the two parts efficiently welded together and the original tensile strength (defect-free bar) could be partly recovered. The defect-free control samples (Fig. 7b) resulted in a tensile strength of 11.2 MPa and an ultimate elongation of 46%. In contrast, the tensile strength of the sample, which contained the hole, was drastically reduced to 2.3 MPa with an elongation of 27.9%.

Due to the thermally triggered repair process, the tensile strength could be regained to a large extend (8.1 MPa), whilst

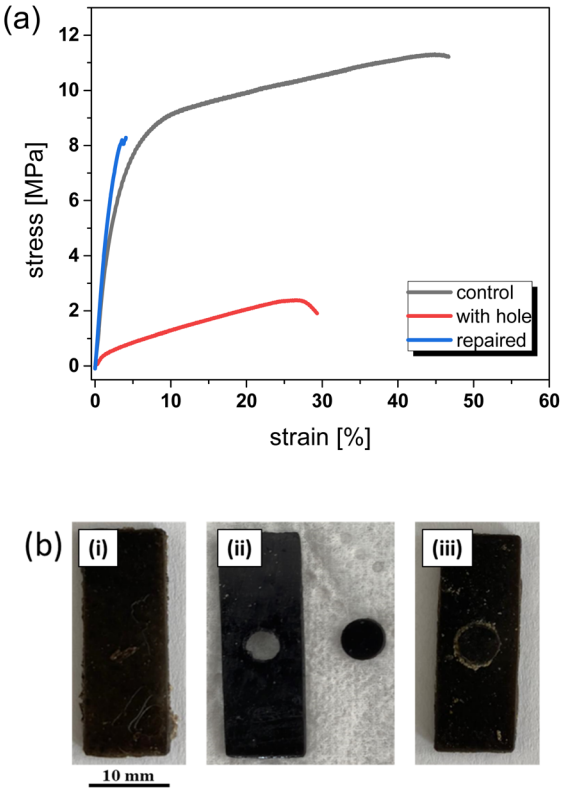

Fig. 7 (a) Stress–strain curves of test specimens DLP 3D-printed with resin-2 containing 4 wt% of Fe_3O_4 nanoparticles prior to and after a thermal healing at 180 °C for 4 h, (b) DLP 3D-printed test specimen used for thermal healing experiments: (i) DLP 3D-printed control sample. (ii) DLP 3D-printed test specimen with a circular-shaped hole in the center and DLP 3D-printed circular shaped counterpart. (iii) Test specimen after fitting the circular-shaped counterpart in the hole and subsequent thermal treatment.

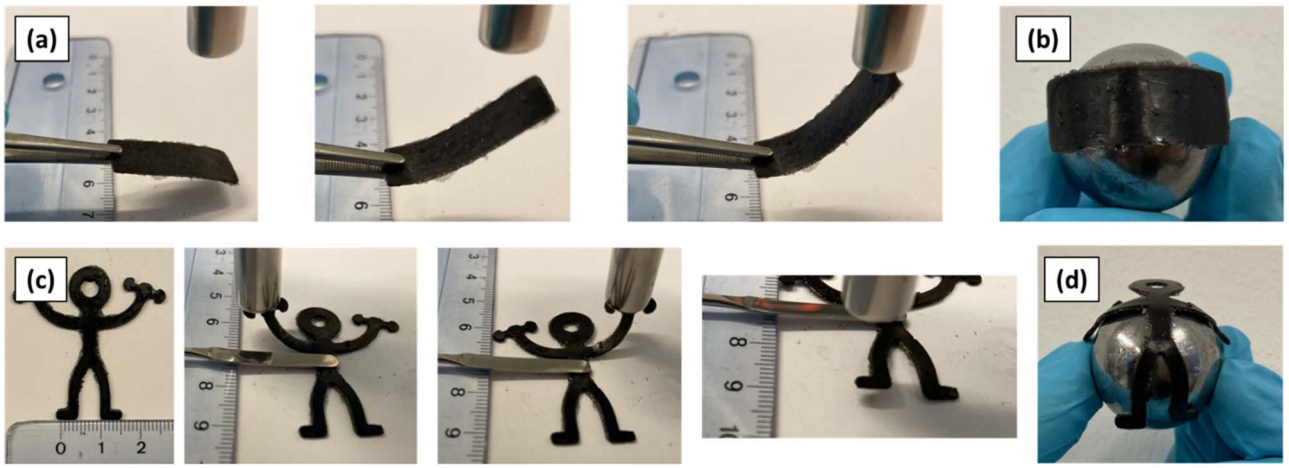

Fig. 6 Activation of objects DLP 3D-printed with resin-2 containing 4 wt% of Fe_3O_4 nanoparticles.

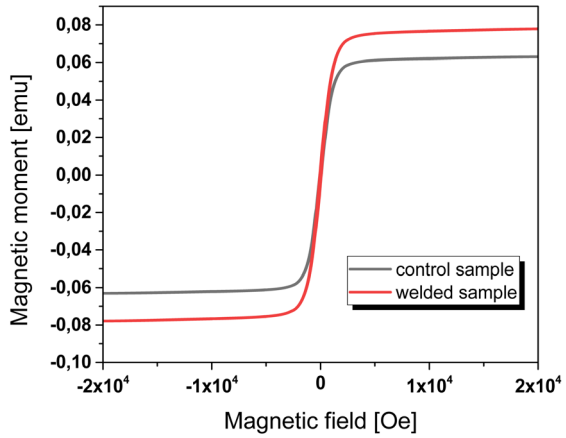

Fig. 8 Room temperature hysteresis loops of 3D-printed magnetic composites from resin-2-4NPs prior to and after welding at 180 °C for 4 h.

the elongation (3.9%) was even lower than the value measured for the sample containing the hole. Whilst the test bars were breaking nearly in the center (Fig. S2 in ESI†), the fracture behavior changed. Since this behavior was not observed in our previous studies on the healing of unfilled dynamic photopolymer networks, we assume that this change in damage behavior is mainly related to the fillers present in the dynamic thiol-acrylate composite.

Along with mechanical performance, the magnetic properties were determined prior to and after thermally induced welding. Room-temperature hysteresis loops of 3D-printed control and welded samples are shown in Fig. 8. The hysteresis curves and the magnetic characteristics of both types of samples (control and welded) are comparable. The coercivities are around 80 Oe (control sample) and 75 Oe (welded sample). Due to the low coercivity at room temperature, one can assume a superparamagnetic behavior, which does not change due to the thermo-activated healing process. The results indicate that the magnetic properties are not affected by the thermal healing step, which has been carried out at 180 °C for 4 h.

3. Experimental

3.1 Material and chemicals

2-Hydroxy-2-phenoxypropyl acrylate (**HPPA**), glycerol 1,3-diglycerolate diacrylate (**GDGDA**), trimethylolpropane tri(3-mercaptopropionate) (**TMPMP**), Fe(II,III) oxide nanoparticles (d_{50} = 50 nm), and phenylbis(2,4,6-trimethylbenzoyl) phosphine oxide (**BAPO**) were purchased from Sigma-Aldrich. **Miramer A99** was used as stabilizer and transesterification catalyst, and was received from Miwon Speciality Chemical (Korea). All chemicals were used without further purification.

3.2 Preparation of resins

3.2.1 Preparation of resin-1. **HPPA** (50 mol%) was mixed with **GDGDA** (25 mol%) and 5 wt% **Miramer A99**. 0.05 wt% Sudan II was added and the formulation was ultra-sonicated until the photoabsorber was dissolved. 3 wt% phenylbis(2,4,6-trimethylbenzoyl)phosphine oxide and **TMPMP** (25 mol%) were added and dissolved by stirring the formulation at room temperature for 30 min.

3.2.2 Preparation of resin-2. **HPPA** (65 mol%) was mixed with **GDGDA** (25 mol%) by means of a magnetic stirrer at room temperature. Subsequently, 5 wt% of phenylbis(2,4,6-trimethylbenzoyl) phosphine oxide and 5 wt% **Miramer A99** were added and the formulations were ultra-sonicated at 40 °C until all components were dissolved. After cooling to room temperature, **TMPMP** (10 mol%) and Fe_3O_4 nanoparticles were added. The prepared formulation was manually stirred with a spatula and sonicated for 1 min at room temperature.

3.3 Characterization

Fourier transform infrared spectroscopy was studied on a Vertex 70 spectrometer (Bruker, USA). Spectra were taken in transmittance mode over a wavenumber range from 4000 to 700 cm^{-1}. All spectra were accumulated from 16 scans at a resolution of 4 cm^{-1} and the absorption peak areas were calculated with OPUS software. For sample preparation, 1.5 μL of resin was drop cast between two CaF_2 discs. Samples were irradiated with a light emitting diode lamp (zgood® wireless LED curing lamp) with a power density of 3.3 mW cm^{-2} (λ = 420–450 nm). The conversion at corresponding exposure times were calculated with OPUS software by evaluating the decrease of the characteristic acrylate infrared absorption band at 1620–1636 cm^{-1}.

The viscosity of the formulations was determined with a modular compact rheometer MCR 102 from Anton Paar (Austria) in a parallel plate set up with a 25 mm diameter. Each measurement was carried out with 0.5 mL formulation at room temperature and a shear rate ranging between 0.1 and 300 s^{-1}. The same measuring setup was utilized to determine the stability of the resins by applying a shear rate of 300 s^{-1} over 14 min.

Dynamic mechanical analysis (DMA) was carried out on a Mettler Toledo DMA/SDTA861e analyzer. Mechanical loss factors ($\tan\delta$) and storage moduli (E') were monitored over a temperature range from −25 to 70 °C at a heating rate of 3 °C min^{-1}, with a frequency of 1 Hz, in a displacement-controlled mode with maximum amplitude 10 μm and maximum force of 5 N. The glass transition temperature (T_g) was determined by the temperature at the maximum of the loss factor. For sample preparation, test specimen (30 mm × 4 mm × 1 mm) were 3D printed with resin-2 using a commercial printer from Anycubic (China).

Mechanical properties were characterized by a ZwickRoell (Germany) Z1.0 static materials testing machine with a crosshead speed of 250 mm min^{-1}. Tensile tests were performed on 3D printed dumbbell specimens (resin-2 filled with 4 wt% nanoparticles) with the dimensions of 2 × 12.5 × 75 mm.

Stress relaxation experiments were carried out at 180 °C on an Anton Paar Physica MCR 501 rheometer (Austria) with parallel plate geometry. Printed samples (10 × 1 mm) of resin-2 were equilibrated to the set temperature and a specified constant normal force of 20 N was applied for 15 min.

Subsequently, 3% step strain was applied and the decreasing stress was recorded over time.

3.4 DLP 3D printing

3D printing was performed on an Anycubic Photo Mono printer (China) with a LED 405 m light source. Two bottom layers were exposed for 24 s, whereas the other layers were illuminated for 5 s. The layer height was set to 50 μm with a building speed of 6 mm s^{-1} and a retracting speed of 1 mm s^{-1}.

3.5 Thermo-activated healing

Both, the control sample and the defect sample with a hole had dimensions of 30 × 10 × 1.5 mm and were printed together with the corresponding disc (d = 5 mm) *via* DLP 3D printing using resin-2 filled with 4 wt% of nanofillers. For the thermal healing, the printed disc was fitted inside the hole and the samples were heated to 180 °C for 4 h.

3.6 Welding experiments and magnetic properties

Three discs (10 × 1 mm) were printed with resin-2 containing 4 wt% of nanofillers. Welding of two discs was achieved by pressing the discs over each other and heating at 180 °C for 4 h. Magnetic properties of control and welded samples were measured with a vibrating sample magnetometer (8600 Series VSM System, Lake Shore) at room temperature. The magnetic field was applied perpendicular to the sample surface in a range between ±1 T.

4. Conclusions

In summary, we have prepared DLP 3D printable thiol-acrylate resins containing magneto-active fillers and dynamic covalent bonds, which rendered the cured photopolymers malleable and thermally mendable. Whilst viscosity and T_g increased with rising filler content, the cure kinetics decreased due to the competition between the nanofiller and the photoinitiator resulting in a slight delay in the photopolymerization process. At a concentration of 4 wt% nanofillers, objects with a simple geometry could be DLP 3D printed and their activation by an external magnetic field was demonstrated. Due to thermo-activated transesterifications, the photopolymers were weldable and thermally healable. Both control and welded samples showed supermagnetic behavior after thermal treatment at 180 °C for 4 hours and the magnetic properties did not significantly change during the welding step. In addition, thermal healing of printed test bars was demonstrated giving rise to the versatility and functionality of the developed resin system.

Conflicts of interest

There are no conflicts to declare.

Acknowledgements

The research work was performed within the COMET-Module project “Chemitecture” (project-no. 21647048) at the Polymer Competence Center Leoben GmbH (PCCL, Austria) within the framework of the COMET-program of the Federal Ministry for Transport, Innovation and Technology and the Federal Ministry for Digital and Economic Affairs with contributions by Montanuniversitaet Leoben, Politecnico di Torino, Helios TBLUS and bto-epoxy. Funding is provided by the Austrian Government and the State Government of Styria. In addition, the authors thank David Reisinger (PCCL) for performing stress-relaxation experiments and Walter Alabiso (PCCL) for carrying out the DMA measurements.

References

1 (*a*) J. Saroia, Y. Wang, Q. Wei, M. Lei, X. Li, Y. Guo and K. Zhang, *Int. J. Adv. Manuf. Technol.*, 2020, **106**, 1695–1721; (*b*) S. C. Ligon, R. Liska, J. Stampfl, M. Gurr and R. Mülhaupt, *Chem. Rev.*, 2017, **117**, 10212–10290; (*c*) M. Hofmann, *ACS Macro Lett.*, 2014, **3**, 382–386; (*d*) M. Nadgorny and A. Ameli, *ACS Appl. Mater. Interfaces*, 2018, **10**, 17489–17507.

2 (*a*) B. C. Gross, J. L. Erkal, S. Y. Lockwood, C. Chen and D. M. Spence, *Anal. Chem.*, 2014, **86**, 3240–3253; (*b*) R. L. Truby and J. A. Lewis, *Nature*, 2016, **540**, 371–378; (*c*) T. D. Ngo, A. Kashani, G. Imbalzano, K. T. Q. Nguyen and D. Hui, *Composites, Part B*, 2018, **143**, 172–196; (*d*) B. Cao, N. Boechler and A. J. Boydston, *Polymer*, 2018, **152**, 4–8.

3 (*a*) W. Associates, *Wohlers report 2016. 3D printing and additive manufacturing state of the industry : annual worldwide progress report*, Wohlers Associates, Fort Collins (Colo.), 2016; (*b*) N. Shahrubudin, T. C. Lee and R. Ramlan, *Procedia Manuf.*, 2019, **35**, 1286–1296.

4 S. Tibbits, *Archit. Design*, 2014, **84**, 116–121.

5 (*a*) A. Ahmed, S. Arya, V. Gupta, H. Furukawa and A. Khosla, *Polymer*, 2021, **228**, 123926; (*b*) Z. Zhang, K. G. Demir and G. X. Gu, *Int. J. Smart Nano Mater.*, 2019, **10**, 205–224; (*c*) M. Y. Khalid, Z. U. Arif, R. Noroozi, A. Zolfagharian and M. Bodaghi, *J. Manuf. Process.*, 2022, **81**, 759–797.

6 A. Kotikian, R. L. Truby, J. W. Boley, T. J. White and J. A. Lewis, *Adv. Mater.*, 2018, **30**, 1706164.

7 H. Yang, W. R. Leow, T. Wang, J. Wang, J. Yu, K. He, D. Qi, C. Wan and X. Chen, *Adv. Mater.*, 2017, **29**, 1701627.

8 Z. Ding, C. Yuan, X. Peng, T. Wang, H. J. Qi and M. L. Dunn, *Sci. Adv.*, 2017, **3**, e1602890.

9 (*a*) A. Lendlein and S. Kelch, *Angew. Chem., Int. Ed.*, 2002, **41**, 2034–2057; (*b*) D. Crespy and R. M. Rossi, *Polym. Int.*, 2007, **56**, 1461–1468.

10 (*a*) A. S. Gladman, E. A. Matsumoto, R. G. Nuzzo, L. Mahadevan and J. A. Lewis, *Nat. Mater.*, 2016, **15**, 413–418; (*b*) J. J. Schwartz and A. J. Boydston, *Nat. Commun.*, 2019, **10**, 791; (*c*) H. Meng and G. Li, *Polymer*, 2013, **54**, 2199–2221; (*d*) Y. Dong, S. Wang, Y. Ke, L. Ding, X. Zeng, S. Magdassi and Y. Long, *Adv. Mater. Technol.*, 2020, **5**, 2000034.

11 R. Marcombe, S. Cai, W. Hong, X. Zhao, Y. Lapusta and Z. Suo, *Soft Matter*, 2010, **6**, 784–793.

12 (*a*) Z. Varga, G. Filipcsei, A. Szilágyi and M. Zrínyi, *Macromol. Symp.*, 2005, **227**, 123–134; (*b*) M. Hossain, D. K. Vu and

P. Steinmann, *Arch. Appl. Mech.*, 2015, **85**, 523–537; (*c*) G. Li, X. Chen, F. Zhou, Y. Liang, Y. Xiao, X. Cao, Z. Zhang, M. Zhang, B. Wu, S. Yin, Y. Xu, H. Fan, Z. Chen, W. Song, W. Yang, B. Pan, J. Hou, W. Zou, S. He, X. Yang, G. Mao, Z. Jia, H. Zhou, T. Li, S. Qu, Z. Xu, Z. Huang, Y. Luo, T. Xie, J. Gu, S. Zhu and W. Yang, *Nature*, 2021, **591**, 66–71.

13 (*a*) M. Sitti, *Nat. Rev. Mater.*, 2018, **3**, 74–75; (*b*) A. K. Bastola and M. Hossain, *Mater. Des.*, 2021, **211**, 110172; (*c*) L. V. Nikitin, D. G. Korolev, G. V. Stepanov and L. S. Mironova, *J. Magn. Magn. Mater.*, 2006, **300**, e234–e238; (*d*) K. Zimmermann, V. A. Naletova, I. Zeidis, V. A. Turkov, E. Kolev, M. V. Lukashevich and G. V. Stepanov, *J. Magn. Magn. Mater.*, 2007, **311**, 450–453; (*e*) P. V. Komarov, P. G. Khalatur and A. R. Khokhlov, *Polym. Adv. Technol.*, 2021, **32**, 3922–3933; (*f*) L. Vítková, L. Musilová, E. Achbergerová, R. Kolařík, M. Mrlík, K. Korpasová, L. Mahelová, Z. Capáková and A. Mráček, *Int. J. Mol. Sci.*, 2022, **23**, 9633.

14 A. K. Bastola, N. Rodriguez, M. Behl, P. Soffiatti, N. P. Rowe and A. Lendlein, *Mater. Des.*, 2021, **202**, 109515.

15 M. Mrinalini and S. Prasanthkumar, *ChemPlusChem*, 2019, **84**, 1103–1121.

16 (*a*) S. Li, H. Bai, R. F. Shepherd and H. Zhao, *Angew. Chem., Int. Ed.*, 2019, **58**, 11182–11204; (*b*) D. Schönfeld, D. Chalissery, F. Wenz, M. Specht, C. Eberl and T. Pretsch, *Molecules*, 2021, **26**, 522; (*c*) L. Hines, K. Petersen, G. Z. Lum and M. Sitti, *Adv. Mater.*, 2017, **29**, 1603483.

17 X. Kuang, D. J. Roach, J. Wu, C. M. Hamel, Z. Ding, T. Wang, M. L. Dunn and H. J. Qi, *Adv. Funct. Mater.*, 2019, **29**, 1805290.

18 (*a*) X. Liu, J. Liu, S. Lin and X. Zhao, *Mater. Today*, 2020, **36**, 102–124; (*b*) M. Cianchetti, C. Laschi, A. Menciassi and P. Dario, *Nat. Rev. Mater.*, 2018, **3**, 143–153; (*c*) A. Lendlein and O. E. C. Gould, *Nat. Rev. Mater.*, 2019, **4**, 116–133; (*d*) Y. S. Lui, W. T. Sow, L. P. Tan, Y. Wu, Y. Lai and H. Li, *Acta Biomater.*, 2019, **92**, 19–36.

19 (*a*) R. Ahamed, S.-B. Choi and M. M. Ferdaus, *J. Intell. Mater. Syst. Struct.*, 2018, **29**, 2051–2095; (*b*) Q. Cao, Q. Fan, Q. Chen, C. Liu, X. Han and L. Li, *Mater. Horiz.*, 2020, **7**, 638–666; (*c*) K. J. Merazzo, A. C. Lima, M. Rincón-Iglesias, L. C. Fernandes, N. Pereira, S. Lanceros-Mendez and P. Martins, *Mater. Horiz.*, 2021, **8**, 2654–2684; (*d*) M. Rafiee, R. D. Farahani and D. Therriault, *Adv. Sci.*, 2020, **7**, 1902307.

20 (*a*) M. R. Jolly, J. D. Carlson and B. C. Muñoz, *J. Intell. Mater. Syst. Struct.*, 1996, **5**, 607–614; (*b*) J. D. Carlson and M. R. Jolly, *Mechatronics*, 2000, **10**, 555–569.

21 (*a*) P. Allia, G. Barrera, P. Tiberto, T. Nardi, Y. Leterrier and M. Sangermano, *J. Appl. Phys.*, 2014, **116**, 113903; (*b*) J. Amici, P. Allia, P. Tiberto and M. Sangermano, *Macromol. Chem. Phys.*, 2011, **212**, 1629–1635; (*c*) C. Albornoz, E. E. Sileo and S. E. Jacobo, *Phys. B*, 2004, **354**, 149–153; (*d*) Q. Ze, X. Kuang, S. Wu, J. Wong, S. M. Montgomery, R. Zhang, J. M. Kovitz, F. Yang, H. J. Qi and R. Zhao, *Adv. Mater.*, 2020, **32**, e1906657; (*e*) T. N. Do, H. Phan, T. -Q. Nguyen and Y. Visell, *Adv. Funct. Mater.*, 2018, **28**, 1800244; (*f*) S. Di Zhang, Y. C. Zhai and Z. F. Zhang, *AMR*, 2011, **287–290**, 2032–2035.

22 (*a*) M. A. Moreno, J. Gonzalez-Rico, M. L. Lopez-Donaire, A. Arias and D. Garcia-Gonzalez, *J. Magn. Magn. Mater.*, 2021, **224**, 109148; (*b*) A. K. Bastola and M. Hossain, *Composites, Part B*, 2020, **200**, 108348; (*c*) A. Hooshiar, A. Payami, J. Dargahi and S. Najarian, *Mech. Syst. Signal Process.*, 2021, **161**, 107918.

23 (*a*) S. Xuan, Y. Xu, T. Liu and X. Gong, *Int. J. Smart Nano Mater.*, 2015, **6**, 135–148; (*b*) Y. Xu, G. Liao and T. Liu, in *Nanofluid Flow in Porous Media*, ed. M. Sheikholeslami Kandelousi, S. Ameen, M. Shaheer Akhtar and H.-S. Shin, IntechOpen, 2020.

24 (*a*) L. A. Makarova, Y. A. Alekhina, A. S. Omelyanchik, D. Peddis, V. V. Spiridonov, V. V. Rodionova and N. S. Perov, *J. Magn. Magn. Mater.*, 2019, **485**, 413–418; (*b*) M. D'Auria, D. Davino, R. Pantani and L. Sorrentino, *Smart Mater. Struct.*, 2016, **25**, 55014.

25 A. Hodaei, O. Akhlaghi, N. Khani, T. Aytas, D. Sezer, B. Tatli, Y. Z. Menceloglu, B. Koc and O. Akbulut, *ACS Appl. Mater. Interfaces*, 2018, **10**, 9873–9881.

26 (*a*) A. Dey, I. N. Roan Eagle and N. Yodo, *J. Manuf. Mater. Process.*, 2021, **5**, 69; (*b*) M. A. S. R. Saadi, A. Maguire, N. T. Pottackal, M. S. H. Thakur, M. M. Ikram, A. J. Hart, P. M. Ajayan and M. M. Rahman, *Adv. Mater.*, 2022, **34**, e2108855.

27 J. J. Restrepo and H. A. Colorado, *J. Compos. Mater.*, 2020, **54**, 647–657.

28 Y. Kim, H. Yuk, R. Zhao, S. A. Chester and X. Zhao, *Nature*, 2018, **558**, 274–279.

29 A. Amirov, A. Omelyanchik, D. Murzin, V. Kolesnikova, S. Vorontsov, I. Musov, K. Musov, S. Khashirova and V. Rodionova, *Processes*, 2022, **10**, 2412.

30 (*a*) D. Kokkinis, M. Schaffner and A. R. Studart, *Nat. Commun.*, 2015, **6**, 8643; (*b*) A. K. Bastola, M. Paudel and L. Li, *Polymer*, 2018, **149**, 213–228; (*c*) L. Lu, P. Guo and Y. Pan, *J. Manuf. Sci. Eng.*, 2017, **139**, 071008.

31 (*a*) E. M. Palmero, J. Rial, J. de Vicente, J. Camarero, B. Skårman, H. Vidarsson, P.-O. Larsson and A. Bollero, *Sci. Technol. Adv. Mater.*, 2018, **19**, 465–473; (*b*) C. Huber, C. Abert, F. Bruckner, M. Groenefeld, S. Schuschnigg, I. Teliban, C. Vogler, G. Wautischer, R. Windl and D. Suess, *Sci. Rep.*, 2017, **7**, 9419.

32 (*a*) J. A. Cuenca, K. Bugler, S. Taylor, D. Morgan, P. Williams, J. Bauer and A. Porch, *J. Condens. Matter Phys.*, 2016, **28**, 106002; (*b*) J. H. Kim, S. Lee, M. Wajahat, H. Jeong, W. S. Chang, H. J. Jeong, J.-R. Yang, J. T. Kim and S. K. Seol, *ACS Nano*, 2016, **10**, 8879–8887.

33 S. Lantean, G. Barrera, C. F. Pirri, P. Tiberto, M. Sangermano, I. Roppolo and G. Rizza, *Adv. Mater. Technol.*, 2019, **4**, 1900505.

34 (*a*) S. Lantean, I. Roppolo, M. Sangermano, M. Hayoun, H. Dammak and G. Rizza, *Addit. Manuf.*, 2021, **47**, 102343; (*b*) S. Lantean, I. Roppolo, M. Sangermano, M. Hayoun, H. Dammak, G. Barrera, P. Tiberto, C. F. Pirri, L. Bodelot and G. Rizza, *Adv. Mater. Technol.*, 2022, **7**, 2200288.

35 E. Rossegger, R. Höller, K. Hrbinič, M. Sangermano, T. Griesser and S. Schlögl, *Adv. Eng. Mater.*, 2022, 2200749.

36 E. Rossegger, R. Höller, D. Reisinger, J. Strasser, M. Fleisch, T. Griesser and S. Schlögl, *Polym. Chem.*, 2021, **12**, 639–644.
37 C. Hinczewski, S. Corbel and T. Chartier, *Rapid Prototyp. J.*, 1998, **4**, 104–111.
38 J.-H. Lee, C.-M. Um and I.-b. Lee, *Dent. Mater.*, 2006, **22**, 515–526.
39 A. Huber, A. Kuschel, T. Ott, G. Santiso-Quinones, D. Stein, J. Bräuer, R. Kissner, F. Krumeich, H. Schönberg, J. Levalois-Grützmacher and H. Grützmacher, *Angew. Chem., Int. Ed.*, 2012, **51**, 4648–4652.
40 (*a*) M. Sangermano, W. Carbonaro, G. Malucelli and A. Priola, *Macromol. Mater. Eng.*, 2008, **293**, 515–520; (*b*) E. Rossegger, D. Nees, S. Turisser, S. Radl, T. Griesser and S. Schlögl, *Polym. Chem.*, 2020, **11**, 3125–3135.
41 (*a*) N. B. Cramer and C. N. Bowman, *J. Polym. Sci., Part A: Polym. Chem.*, 2001, **39**, 3311–3319; (*b*) M. Sahin, S. Ayalur-Karunakaran, J. Manhart, M. Wolfahrt, W. Kern and S. Schlögl, *Adv. Eng. Mater.*, 2017, **19**, 1600620.